Texture Characterization of Chemically Prepared Toners

Kevin Lofftus, Eastman Kodak Company, Rochester NY/USA

Abstract

Texture of toners affects many electrophotogaphic properties. The limited coalescence manufacturing method used to make chemically prepared toner (CPT) results in folded spheres with complex shapes. The thickness and quantity of these folds may be assessed by the amplification of light scattering. Evaluation of SEM photomicrographs shows a correlation of the fold thickness and light-scattering amplification. The angular scattering information indicates that the amplification occurs over all size scales rather than that of the fold thickness. Other texture information may be gathered from surface area and the cavity volume included in the folds. The included cavity volume of the folds may be assessed by the combination of spherical equivalent and aerodynamic diameters.

Introduction

Toner texture influences particle cohesiveness and integrity as well as adhesion to substrates. Chemically prepared toner (CPT) made using the evaporative limited coalescence (ELC) manufacturing process [1] is capable of producing a variety of textures. The texture of the CPT can be varied from smooth to a variety of highly folded by changing process conditions and shape control additive (SCA) level and type. Textures produced by ELC are significantly different from those of melt-pulverized toners (MPT). These differences lead to different performances in electrophotographic processes.

Background

Texture is difficult to quantify. Most shape characteristics attempt to describe an ensemble of three-dimensional particles with a few statistics from a distribution that describe one or two dimensions. Previous image analysis methods have defined several shape factors that characterize shape and texture. Examples of shape factors are SF1, SF2, and SF5 [2].

SF1 is the ratio of the circular area defined by the longest dimension between tangents L_{max} to the projected area A_p:

$$SF1 = 100\,\pi L_{\max}^2 / \left(4A_p\right). \quad (1)$$

This shape factor is related to the (inverse) aspect ratio R_b measured by the Sysmex FPIA3000. The Sysmex defines the max distance aspect ratio as the distance between tangents $L_{max,v}$ that are perpendicular to L_{max} divided by L_{max}. It is obvious from Eq. 1 that SF1 divided by 100 times semi-major axis aspect ratio (R_b = $L_{max,v}/L_{max}$) is equal to one for ellipses and circles and is less than one for other shapes. Defining this ratio as the elliptical roundness R_E allows one to characterize the particle texture on the scale of the particle radius. Sysmex selects the corners of squares and rectangles to determine L_{max} and R_E is $\pi/4$ for these shapes. R_E becomes even smaller for star-shaped perimeters. In previous work [3, 4], CPT's made by ELC were modeled by ellipsoids where the major axis a is taken as L_{max} and the semi-major axis b as $L_{max,v}$, and the minor axis c computed from combined Multisizer and Sysmex measurements.

Shape factors SF2 and SF5 characterize roughness or texture. SF2 is the ratio of the circular area defined by the perimeter P to the projected area A_p while SF5 is the ratio of the perimeter to the convex hull perimeter P_x:

$$SF2 = 100\,P^2 / \left(4\pi A_p\right). \quad (2)$$

$$SF5 = 100P / P_x\,. \quad (3)$$

SF5 characterizes only the roughness at the perimeter while SF2 mixes the aspect ratio of the particle with roughness. For SF5 to be greater than 100, P must be greater than P_x. This it true only if there are apparent concavities at the particle image edge. It was shown that sharp folds generate bright spots at the edge of a particle image that are interpreted as concavities by image analysis using a Sysmex FPIA3000 [3].

Light scattering may be used to evaluate the fold and cavity dimensions. Constructive interference increases the amount of light scattered. It occurs at resonance frequencies where the difference in path lengths from each sidewall of a fold or cavity to a point far away from the particle is an even multiple of the wavelength. The light scattered is also a strong function of the scattering angle. Most of the light scattered by a structure of thickness T occurs at angles less than $\pi nT/10\lambda$ [5]. The total scattering is the integration of the scattering paths over all scattering directions times the total area of the folds. The scale of texture characterized by light scattering is that of the first resonance.

The first resonance of red laser light was found to be 1.85 μm for spherical toners in water based upon Mie calculations using the algorithm of Bohren and Huffman [6]. The total extinction coefficient C_{ext} is asymptotic to two times the projected area for very large particles. Resonances can be both constructive and destructive causing a ringing around a level of two. For toners that are relatively transparent to the measurement wavelength, the constructive interference amplifies C_{ext} to factor of 3.6 of that of the projected area. Also, there is a second resonance at 4.94 μm with an amplification factor of 2.6 and a minimum at 3.40 μm that has an amplification factor of 1.6. For particles largely opaque to the wavelength of light, there is only one weak resonance at 1.75 μm with an amplification factor of about 2.6. This ringing in transparent materials confounds light scattering from structures larger than the first resonance with those below it. For scattering structures below the size of the first resonance, the amount of light scattered will be dependent on both the size and the total area of the scattering structure. Therefore, a measure of the total area of the structures is needed to evaluate the thickness of these structures.

The surface area of toners may be evaluated the by Brunauer, Emmett, and Teller method (BET) of evaluating surface area of

powders by multilayer gas adsorption [7]. The surface areas of CPT's are near the lower limit of resolution for commercially available instruments when nitrogen is used as the adsorbate gas. An adsorbate gas with a liquefaction temperature significantly higher than the adsorption temperature can improve accuracy for systems that evaluate surface area by measuring changes in pressure as a fixed volume of gas is adsorbed. The difference in measured surface area from that expected for a smooth ellipsoid can be used to evaluate the area of the scattering structure of textured CPT's. The elliptical equivalent surface area may be approximated [8] by

$$S_e = 2\pi\left(c^2 + abg + \frac{b^2 - c^2}{3ab} g^3 h \right) \quad where$$
$$g = \cos^{-1}(a/c) \Big/ \sqrt{1 - a^2/c^2} \tag{4}$$
$$h = c^2 - \frac{a^2}{2} + \frac{\left(a^4 b^2 + 3a^4 c^2 - 12a^2 c^4 + 8b^2 c^4\right) g^2}{40 a^2 b^2}$$

to avoid evaluating the incomplete elliptic integrals of the first (E) and second (F) kind in Legendre's expression [9]

$$S_e = 2\pi\left(c^2 + \frac{ab}{\sin(t)} \left(\cos^2(t) E\left(t, k^2\right) + \sin^2(t) F\left(t, k^2\right) \right) \right) \tag{5}$$
$$where$$
$$t = \cos^{-1}(c/a), \quad s = \cos^{-1}(c/b), \quad k = \frac{\sin(s)}{\sin(t)}$$

Another approach in evaluating the area of the scattering structure is to characterize the cavity volume. The convex hull volume may be estimated from size measurements based upon particle drag in a fluid. Generally, the fluid will not flow through the cavities and the combined volume is measured. The cavity volume may be expressed as porosity and is related to the amount of surface area that amplifies light scattering, the tendency for particles to interlock, and particle integrity.

Materials and Methods

A single dispersion of each pilot scale CPT was made at 0.200% in water using a mixture of ionic and nonionic surfactants [10] and was measured on a FPIA3000 from Malvern Instruments Inc., a Mastersizer 2000 from Malvern Instruments Inc., and on a Multisizer 3 from Beckman Coulter Inc. Dry samples were measured on an Aerosizer Mach 2 from Amherst Process Instrument Inc. with an aerodisperser dry powder feed unit. BET surface areas were measured on selected samples at Micromeritics Inc. using a TriStar II 3020.

The measurements were reduced to texture characteristics which were correlated to performance in Kodak NexPress digital production color presses. Image quality metrics were used to assess performance affected by adhesion to surfaces in the printer. Poor performance was characterized by adhesion metrics that were greater than twice the nominal level. Particle integrity was evaluated by observing contamination of cylinders and rolls where forces are applied that may cause fragmentation.

Measurements in the FPIA3000 and the Multisizer are described elsewhere [4]. The Sysmex FPIA3000 allows for six joint distributions between a size factor and a form factor in one standard operating procedure. One size factor reported by the Sysmex is the circularly equivalent number diameter D_{CE} that computed from A_p. The joint distributions of R_b with D_{CE}, L_{max}, A_p, P, and P_x from the FPIA3000 were analyzed using 140 R_b bins from 0.3 to 1 and 226 bins on a log scale with ranges of 1 to 25 μm for D_{CE}, 1.2 to 30 μm for L_{max}, 3 to 90 μm for P and P_x and 0.5 to 500 μm^2 for A_p. The joint distribution of R_b with convex hull area A_x was collected in a similar manner as A_p to estimate the limits to match that of the Multisizer for P and P_x (see below).

A calibration is applied to the size factors by the Sysmex software. It was noted that the size correction was not applied uniformly for the different size factors and nonlinear calibrations were developed using calibration beads. Two calibrations were developed, one for L_{max} to D_{CE} and one for A_p to D_{CE}. A calibration relationship between L_{max} and A_p was not readily developed. Therefore, SF1 was calculated using D_{CE} rather than A_p:

$$SF1 = 100\left(L_{\max} / D_{CE}\right)^2 . \tag{1A}$$

Conditional distributions with respect to R_b were calculated for SF1, R_E, SF2, and SF5 at each R_b having 10 or more particles. Number average values were used for texture characterization.

The dynamic range of the Sysmex is greater than that of the Multisizer and the Sysmex data must be limited to match the Multisizer. Additionally, some aggregation in the saline may occur giving some erroneous large particles for the Mulitsizer data that greatly influences the estimated light scattering for spherical equivalent particles (see below). Since the Sysmex analyzes the larger two dimensions of the toner, the limits of the Sysmex data do not directly translate to the Multisizer limits. A method to estimate the D_{SE} equivalent Sysmex D_{CE} size limits was developed to take into account that the minor axis c aspect ratio ($R_c = c/a$) may be a strong function of R_b [4]. The mean D_{CE} and R_b were estimated of each quartile of R_b. The trend of R_c with R_b was found and the D_{CE} size limits for each R_b were calculated using Eq. 3 in reference [4]. These limits were approximated for the other Sysmex size factors except P_x. by using the calibration expressions for L_{max} and A_p to D_{CE}. The limit to P_x was estimated by evaluating A_x limit as described for A_p and applying the factor of $(A_x/A_p)^{1/2}$ to the limit of P for each R_b.

The same sample preparation used for FPIA3000 and Multisizer measurements was measured on a Mastersizer 2000 at five increasing concentrations using the same initial background and adding the same volume of dispersion to the dilution chamber for each consecutive concentration. The exact cumulative weight of the dispersion was recorded and the laser obscuration was measured. A least-squares fit to a line was found for the obscuration divided by the weight of toner in the dispersion added versus that weight. Points statistically outside the line were rejected and the remaining data fit to find the intercept. This intercept represented the scattering effect at infinite dilution per unit weight of toner.

Light scattering from spheres was estimated using the Coulter Multisizer size distribution to interpolate values from a table of Mie calculations. The Mie calculations of C_{ext} were preformed using the algorithm of Bohren and Huffman [6] for a wavelength of 0.6328 μm for a water suspension of particles with real refractive index of n = 1.55 and imaginary refractive indices κ in the set {0, 0.0002, 0.002, 0.01, 0.02, 0.04, 0.08, 0.16, 0.32}. Each calculation was performed for particle diameters ranging from -0.5 to 1.9 log μm in steps of 0.006. Changes in C_{ext} due to changes in refractive index and wavelengths were interpolated as changes in

size using the fact that C_{ext} may be represented by a single curve as a function of λ/nr for a given κ where r is the particle radius. These interpolated results were then interpolated for κ. For cyan CPT's in this study, κ was about 0.05 resulting in a resonance peak of 2.88 at 1.8 μm with substantially no other resonances.

The convex hull volume was evaluated using an Aerosizer Mach 2. This instrument is a counting device that measures time of flight of particles across a fixed spacing in vacuum after accelerating in a nozzle designed to reach supersonic velocities. As the air jet becomes less dense, the drag becomes small and the particles maintain a nearly constant velocity. This velocity is determined by the integrated acceleration in the nozzle due to drag force divided by the inertial force. These forces are dependent on the particle size and density giving a monotonic response with size and density. Shape influences this measurement in several ways. First, the drag is greater in the laminar regime giving greater acceleration in the throat of the nozzle. Second, the slip correction is greater in the low-density supersonic flow reducing drag and acceleration. Finally, Reynolds numbers in the throat of the nozzle may be near 50 [11] causing alignment of the particle in the flow for Reynolds numbers greater than 0.1 [12]. Alignment minimizes drag and reduces acceleration. The latter two effects offset the first effect reducing the impact of shape on the size measurement.

The increased volume of the included cavities increases the drag force accelerating the particles without increasing the inertial resistance resulting in shorter time-of-flight (TOF) response in the instrument. The TOF data is converted to an aerodynamic spherical equivalent diameter D_a using the value of particle density ρ. Since the convex hull volume is not known, the density including the cavity porosity ρ_ε is not known and the measurements were made using the toner density. The combination of the Multisizer D_{SE} and the calibration between time-of-flight and D_a was used to solve for ρ_ε. This calibration was determined over the toner particle size range by measuring spheres and changing the input value of ρ from 0.25 to 4 resulting in a fit of

$$D_{a,\rho_1} / D_{a,\rho_2} = \left(\rho_2 / \rho_1\right)^{0.905}. \quad (6)$$

The Multisizer does not measure the volume of any cavities that are sufficiently open to allow salt ion movement in an electric field. Assuming there are no closed pores, D_{SE} is the correct size to use with the true particle density ρ. The porous aerodynamic diameter $D_{a,e}$ is related to ρ_ε by a mass balance for the particle:

$$(\pi/6) D_{a,\varepsilon}^3 \rho_\varepsilon = (\pi/6) D_{SE}^3 \rho. \quad (7)$$

Eliminating $D_{a,\varepsilon}$ using Eqs. 6 and 7 and solving for ρ_ε., we have

$$\rho_\varepsilon = \rho\left(F_{ca} D_a / D_{SE}\right)^{1/(1/3+0.905)} \quad (8)$$

where F_{ca} is the calibration factor between the Multisizer and the Aerosizer. The results were reported as porosity ε:

$$\varepsilon = \frac{V_\varepsilon - V}{V_\varepsilon} = \frac{\left(1/\rho_\varepsilon - 1/\rho\right)}{1/\rho_\varepsilon} = 1 - \frac{\rho_\varepsilon}{\rho} \quad (9)$$

Dispersion by the aerodisperser resulted in differences in aggregation and fines generation for toners with high porosities and poor particle integrity. To mitigate these differences, the computation of porosity was done using the geometric diameter number modes from the Aerosizer and the Multisizer. These modes were found finding the root of the derivative of a 5th order polynomial least-squares fit as described elsewhere [4].

Results

Many of the texture metrics were found to be correlated within a given set of ELC chemistries and processes. A strong correlation between SF2 and SF5 was obtained. The value of R_E was found to be strongly correlated to SF5 and light scattering when R_b is modified only by SCA level. Process extremes that lead to differences in the R_c distribution often show a difference in the relationships between the texture metrics. The best metric of the R_c distribution to differentiate adhesion performance was found to be the trend of R_c with respect to R_b (dR_c/dR_b).

The various texture metrics and performance evaluations for selected CPT's are presented in Table I for 6 μm toners. A cyan MPT was included for comparison. This MPT was made using the production process for the current cyan toner made by Kodak but at a smaller size and increased pigment loading to match the CPT's. Five cyan CPT's made with variations in process conditions and SCA levels are numbered 1 to 5. Included are a cyan CPT with a different SCA labeled A, a magenta CPT, and a yellow CPT.

Table 1 Texture Metrics and Performance for Selected Toners.

Sample	MPT	1	2	3	4	5	A	Mag.	Yel.
SC Var	NA	Proc	Proc	Proc	Proc	Proc	Chem	Proc	Proc
R_E	0.892	0.910	0.896	0.888	0.921	0.899	0.914	0.897	0.880
SF2-100	10.98	8.90	10.10	13.99	6.34	11.83	7.31	10.55	16.94
SF5-100	1.12	1.93	2.06	3.37	2.33	1.34	1.21	1.99	4.12
LS	1.21	1.44	1.34	1.46	1.71	1.22	1.14	1.39	1.74
S_{BET}/S_e	NA	2.26	2.13	2.77	NA	1.86	1.16	2.71	3.47
ε	0.13	0.24	0.20	0.27	0.25	0.20	0.11	0.27	0.32
dR_c/dR_b	0.11	-0.25	0.06	-0.19	-0.03	0.89	0.37	0.05	-0.10
Flow	Good	Good	Good	Poor	Good	Good	Good	Fair	Poor
Adhesion	Good	Fair	Fair	Good	Fair	Poor	Poor	Fair	Good
Integrity	Good	Good	Poor	Poor	Good	Poor	Good	Poor	Poor

Particle integrity was found to be poor when the folds of the toner were thin and the cavities were open sufficiently that mechanical forces could be applied to these folds. As the amount of folds increases in number, so does the porosity. Light scattering increases with both greater number of folds and increasing fold thicknesses up to 1.7 μm. It was found that the light scattering needed to be above a certain level for a given porosity to have good particle integrity (Figure 1a). Because of the ambiguity of light scattering, there is a region of transition where the particle integrity cannot be determined by light scattering and porosity. The limited set of BET values in Table 1 appears to separate the performance in this region (Figure 1b). The samples 1, 3 and Mag have similar light scattering and porosity characteristics but the latter two have a greater BET and poor integrity. BET also predicted bridging in the replenishment hoppers (Flow in Table 1).

Particle textures that lead to high contact areas are highly adhesive and not readily moved by applied electrostatic and mechanical forces resulting in poor image quality performance. These forces are applied to individual particles making performance susceptible to a small faction of image toner particles,

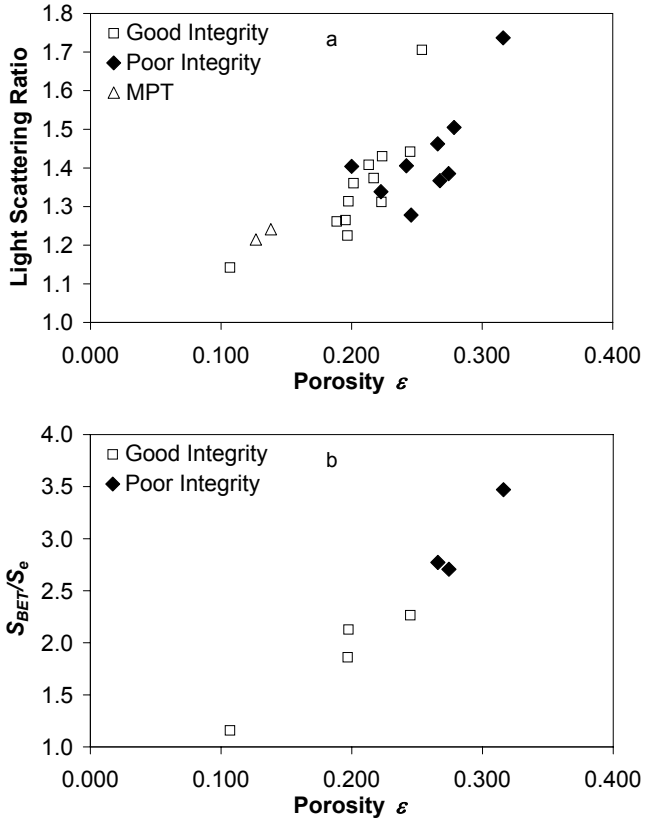

***Figure 1**. Particle integrity as a function of texture characteristics: a) porosity and light scattering ratio, and b) porosity and relative surface area.*

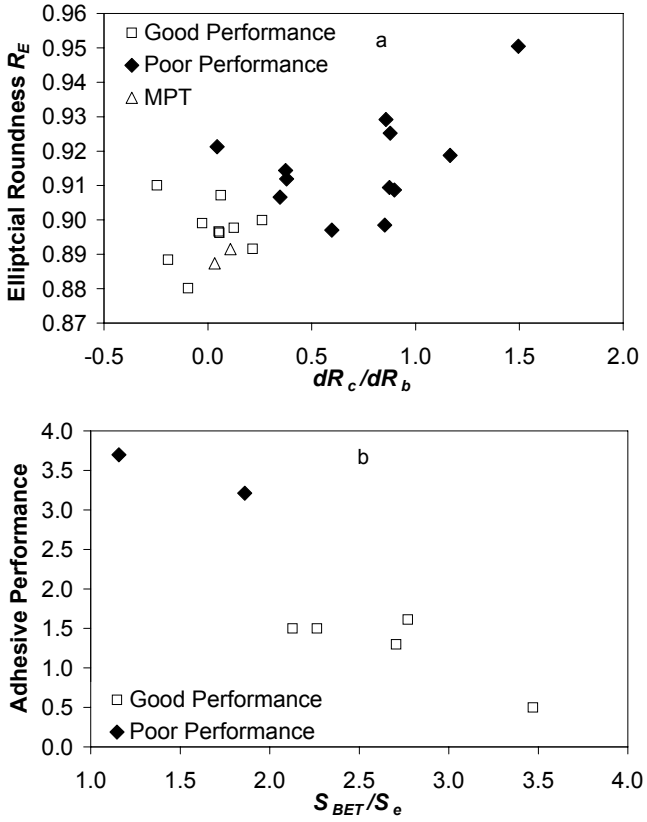

***Figure 2**. Adhesion performance as a function of texture characteristics: a) minor aspect ratio distribution width and elliptical roundness, and b) relative surface area.*

a small fraction of the texture distribution. For narrow texture distributions, the mean texture may correlate well with performance. Broad texture distributions arise from conditions that often lead to broad shape distributions. The strongest correlations to performance were found with R_E for texture and dR_c/dR_b for shape distribution width with good performance defined by $R_E < 0.92\text{-}0.05 dR_c/dR_b$ (Figure 2a). BET also correlates with performance where $S_{BET}/S_e < 2$ gives good performance (Figure 2b).

Conclusion

Elliptical roundness, porosity, and surface area can be used to characterize toner texture that correlate to electrophotographic performance.

References

[1] M. Nair, Z. Pierce, and C. Sreekumar, US Patent 4833060, 1989.

[2] T. Kaysuyu et al., US Patent 6214509, 2001.

[3] K. Lofftus, Extending Toner Shape Analysis to 3D, Proc. NIP23 (IS&T, Fairbanks, A, 2007) pp. 209-212.

[4] K. Lofftus, Distributed 3D Aspect Ratios of Toner, Proc. NIP24 (IS&T, Pittsburg, PA, 2008).

[5] C. F. Bohren and D. R. Huffman, Absorption and Scattering of Light by Small Particles (Willey, New York, NY, 1983) pg. 111.

[6] Ibid., pg. 479.

[7] S. Brunauer, P. H. Emmett, and E. Teller, J. Am. Chem. Soc., 60, 309 (1938).

[8] A. Dieckmann, Universität Bonn, July 2003, http://pi.physik.uni-bonn.de/~dieckman/index.html.

[9] A. Krajcik and K. McLenithan, Integrals and Series Related to the Surface Area of Arbitrary Ellipsoids, Arxiv preprint math/0605216 (2006).

[10] K. Lofftus, Improvements in Toner Fines Characterization, Proc. NIP21 (IS&T, Baltimore, MA, 2005) pp. 484-487.

[11] B. Daneke, Time-of-Flight Aerosol Beam Spectrometer for Particle Size Measurements, EPA-800/2-77-229, National Technical Information Service, US Dept. Comm. (1977), pg. 47.

[12] B. Daneke, "Slip Correction Factors for Nonspherical Bodies--I Introduction and Continuum Flow," Aerosol Sci., 4, 139 (1977).

Author Biography

Kevin Lofftus received a B. S. in 1982 and an M. S. in 1984 for Mineral Process Engineering from Montana College of Mineral Science and Technology and a Ph. D. in 1989 from The University of California Berkeley for Mineral Processing with minors in Chemical Engineering and Statistics. He joined the Copy Products Division of Kodak in 1989 and is currently a Senior Research Scientist at Eastman Kodak Company